A CMOS Electrochemical Biochip With 32 × 32 Three-Electrode Voltammetry Pixels

Arun Manickam, *Member, IEEE*, Kae-Dyi You, Nicholas Wood, Lei Pei, Yang Liu, Rituraj Singh, Nader Gamini, Mark W. McDermott, *Life Member, IEEE*, Davood Shahrjerdi, *Senior Member, IEEE*, Robert G. Kuimelis, and Arjang Hassibi, *Senior Member, IEEE*

***Abstract*— A CMOS-integrated electrochemical biochip for high-performance molecular testing is presented. The system includes an array of 32 × 32 three-electrode voltammetry pixels and on-chip temperature control between 25 and 95 °C. Each 100 μm × 100 μm pixel includes a CMOS-compatible and chemo-stable amorphous carbon electrode transducer connected to in-pixel ΣΔ current detection circuitry with 280 fA rms input-referred noise (0.1–20 Hz bandwidth) and 93 dB dynamic range (DR). Array-based DNA detection assays are implemented, and successful DNA melt-analysis and real-time label-free DNA hybridization detection are reported.**

***Index Terms*— Biochip, biosensor, DNA sequencing, electrochemical, lab-on-chip, microarrays, molecular diagnostics (MDx), nucleic acid, voltammetry.**

I. Introduction

THE use of electronic methods to detect bio-analytes, such as nucleic acids (DNA and RNA), proteins, and small molecules, is one of the cornerstones of the field of biosensors and bioelectronics [1]. Electronic devices and sensor systems, broadly defined, are robust, high performance, manufacturable, and scalable. Hence, they have the potential to become the dominant detection platform for many molecular biosensing applications, where performance, cost-efficiency, and high-volume production are imperative. Example applications include point-of-care (PoC), molecular diagnostics (MDx), food testing, and environmental monitoring.

From the sensor signal chain perspective, electronic (or electrochemical) biosensors are far simpler than their widely used optical (fluorescence and bioluminescence) counterparts [2]–[7]. Electronic biosensors only require electrode–electrolyte interfaces coupled with low-noise front-end current or voltage detection circuitry. This is in contrast to delicate and bulky optical components and narrowband excitation sources necessary for optical systems [8]–[11]. Despite this advantage, the adoption and successful commercialization of electrochemical techniques to detect complex molecules, such as DNA or proteins, have been limited. One can attribute this to three technical challenges. The first is the high interference (background) in electro-analysis, broadly defined, which originates from the electrostatic nature of electrode–electrolyte interfaces [12], [13]. The second is the manufacturing challenge in creating both a chemically stable (inert) and biocompatible electrolyte transducers [14]. The third is the circuit and IC design challenges associated with integrated electroanalytical biosensors, particularly in high-density arrays that are most applicable in the biotechnology space [15].

There are different electrochemical detection techniques, such as voltammetry, charge-based sensing, and impedance spectroscopy [15]. Voltammetry [2]–[6] is perhaps the most popular for biosensing, as it can uniquely take advantage of electro-active molecules [reduction–oxidation (redox) labels] to create target-specific electronic signals that are not possible using other methods that rely on changes in surface charge or impedance changes. It is important to note here that voltammetry is suitable for small-to-medium density arrays (<1000 elements) and integration of high-fidelity front-end detection circuitry to compensate for electrode–electrolyte surface drifts. However, for any higher density arrays that require densely packed transducers (>1M sensing elements), charge-based techniques are the only practical option so far.

In this article, we present a CMOS-integrated electrochemical biochip that is specifically designed to address the above limitations. The system adopts three-electrode voltammetry and redox labeled analytes to increase the signal to background. Amorphous carbon (a-C) electrode transducers are successfully implemented to create manufacturable and biocompatible transducer elements on the back end of the CMOS process [16]. To be precise, the use of a-C surfaces offers an electrically conductive surface to which biosensing probes are covalently attached. This is a major advantage over commonly used precious metal (e.g., Au and Pt) electrodes [2]–[6] with non-covalent probe attachment schemes (e.g., thiol bonds [17]) with thermal stability of <60 °C. From a material perspective, a-C (and carbon in general) is also compatible with conventional VLSI fabrication processes and does not require an isolated back-end process when compared to Au and its device contamination concerns [18].

Manuscript received May 19, 2019; revised August 8, 2019 and August 27, 2019; accepted August 27, 2019. Date of publication October 15, 2019; date of current version October 23, 2019. This article was approved by Guest Editor Pedram Mohseni. *(Corresponding author: Arun Manickam.)*

A. Manickam, N. Wood, L. Pei, Y. Liu, R. Singh, N. Gamini, M. W. McDermott, R. G. Kuimelis, and A. Hassibi are with InSilixa Inc., Sunnyvale, CA 94089 USA (e-mail: arun.manickam@insilixa.com; nicholas.wood@insilixa.com; lei.pei@insilixa.com; yang.liu@insilixa.com; rituraj.singh@insilixa.com; nader.gamini@insilixa.com; mark.mcdermott@insilixa.com; bob.kuimelis@insilixa.com; arjang.hassibi@insilixa.com).

K.-D. You and D. Shahrjerdi are with the Electrical and Computer Engineering Department, New York University, Brooklyn, NY 11201 USA (e-mail: kd.you@nyu.edu; davood@nyu.edu).

Color versions of one or more of the figures in this article are available online at http://ieeexplore.ieee.org.

Digital Object Identifier 10.1109/JSSC.2019.2941020

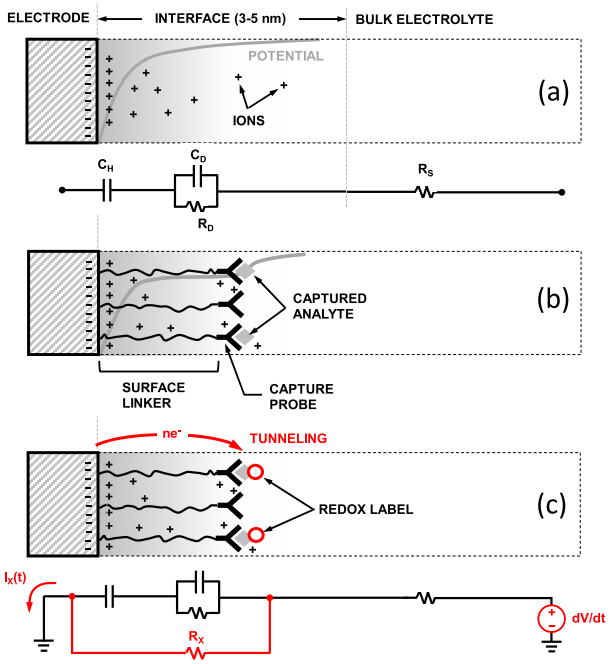

Fig. 1. Electrostatic model, charge distribution, and lumped circuit models of (a) electrolyte–electrolyte half-cell, (b) electrochemical biosensor, and (c) biosensor with redox labeled amplicons during voltammetry.

Finally, a low-noise and high dynamic range (DR) $\Sigma\Delta I-V$ sensor is designed in every pixel to offer a fully integrated high-density programmable signal chain. The usage of $\Sigma\Delta I-V$ sensor permits higher DR detection packed into a small pixel area when compared to other works that employ direct integration or SAR-based scheme [3]–[7]. Furthermore, a 32×32 pixel array, an on-chip three-electrode system, and an integrated thermal control system make our biochip suitable for high multiplex biomolecular assay development. Example applications are in molecular testing, specifically infectious disease, agriculture, biology, water quality, and food testing.

We first discuss in Section II, the system-level architecture of the implemented system and how the IC specifications are derived. In Section III, we describe in detail the IC and electrode implementation, followed by measurement results in Section IV. A conclusion is provided at the end of Section V.

II. Architecture and Specifications

A. Electrode–Electrolyte Transducers

We need to carefully consider the electrostatic nature of electrolyte–electrolyte interfaces to optimize an electrochemical biosensor. In Fig. 1(a), we depict the charge distribution, potential, and circuit model of a half-cell. While the electrolyte bulk and electrode can both be modeled as conductors, the electrode–electrolyte interface model includes two capacitors. As depicted, C_H is an ideal lumped capacitor and it represents the inner layer with immobilized interface ionic charge, and C_D and R_D model the lossy, distributed, and non-linear diffusion capacitance. Typically for unmodified electrode surfaces, $C_H \gg C_D$. C_D can vary between 10 and 100 μF/cm^2 for typical biological conditions with ionic strength varying between 10 and 100 mM. For biosensing, we attach probes to the electrode surface [see Fig. 1(b)], which results in a certain distance (typically <5 nm for biological buffers) between the electrode surface and the captured analyte. Therefore, analyte capturing only perturbs the charge distribution of the diffusion layer. Such perturbations are always relatively small (transduction gain between 10^{-2} and 10^{-4}) and hence difficult to measure, given the sensor additive noise and electrode interface drifts and instability [19].

B. Redox-Based Voltammetry

One solution to the above impediment is to include electrochemical reporters to boost the transduction gain and create a stronger analyte-specific electronic signal. One category of reporters is redox molecular labels. These labels participate in an n electron exchange reaction, i.e., $(O + \mathrm{ne}^- \leftrightarrow R)$ [12], [20], [21], when placed in close proximity to the electrode. If we consider N_t as the total number of redox labels, then the concentration of oxidized labels, N_o, is computed from the Nernst equation [13] as

$$N_o = N_t \frac{\exp\left(\frac{nF}{RT}(V - V_{ox})\right)}{1 + \exp\left(\frac{nF}{RT}(V - V_{ox})\right)} \tag{1}$$

where V is the electrode–electrolyte interface potential, V_{ox} is the standard potential of redox reaction, R is the molar gas constant, F is the faraday constant, and T is the absolute temperature.

Now, in order to detect the labels, we sweep V (perform voltammetry [13]) to create a redox current, I_x, which can be derived from (1) as

$$I_x = \mathrm{ne}\frac{dN_o}{dt} = \mathrm{ne}\frac{dN_o}{dV}\frac{dV}{dt}. \tag{2}$$

As depicted in Fig. 1(c), I_x can be modeled as R_x, a nonlinear (voltage-dependent) resistance that appears only when the labeled analytes are captured by the probes. It is important to recognize that in voltammetry, we not only create the informative I_x but also create a non-informative (background) displacement current, I_b. By assuming that R_D is negligible and the surface is purely capacitive, we can approximate I_b by

$$I_b \approx \frac{C_H C_D}{C_H + C_D}\frac{dV}{dt}. \tag{3}$$

By combining (2) and (3), we can now calculate the intrinsic signal to background of the voltammetry method, which is

$$\frac{I_x}{I_b} \approx \mathrm{ne}\frac{dN_o}{dV}\Big/\frac{C_H C_D}{C_H + C_D}. \tag{4}$$

C. Voltammetry Setup

It is common to adopt potentiostat circuits [22], [23] to generate the required dV/dt of voltammetry, as shown in Fig. 2. In this setup, the electrode where I_x is created is referred to as working (WE), while two other electrodes, the reference (RE) and counter (CE), establish the sweeping potential.

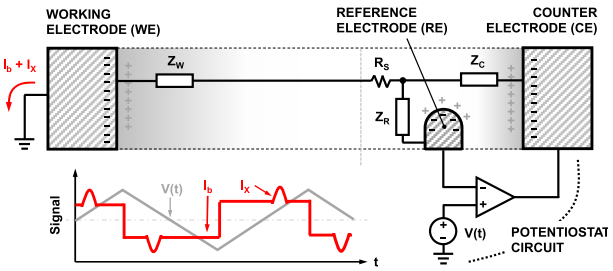

Fig. 2. Circuit model for three-electrode voltammetry system used for general affinity-based biosensing.

TABLE I
BIOCHIP SPECIFICATIONS

Parameter	Value	Justification
Biosensor pixel dimensions	100µm ×100µm	Minimum pitch for high volume surface functionalization
Number of pixels	1000	Multiplexing (< 250 analytes and redundancy of 4)
Operating temperature	25-95°C	Compatibility with DNA-based assays
Reaction volume	50µl	Conventional *In-vitro* diagnostics workflow
Surface probe density	10^3-10^4µm^{-2}	Optimal surface density for analyte target accessibility
Electrode material	Amorphous carbon (a-C)	Manufacturable, chemo-stable and bio-compatible
Electrode setup	3-electrode configuration	High performance voltammetry
Voltage sweep range	±0.75V	High performance voltammetry
Current detection range	0.5pA – 1nA#	Appropriate range for detecting small I_x in large I_b
Detection Bandwidth	1-50Hz	High performance voltammetry
CV Scan Rate	0.1 – 1V/s	High performance voltammetry
WE capacitance	100pF - 1nF#	Varying surface capacitance (10-100µF/cm^2)

#for 1000µm^2 working electrode area

In the ideal case, $R_S \rightarrow 0$, making the error in applied voltage across WE, ΔV, zero. With finite R_S, we have

$$\Delta V = \frac{Z_W R_S}{Z_W + R_S} V \tag{5}$$

where Z_W is the interface impedance of the WE.

It is evident from (5) that we can make $\Delta V \rightarrow 0$ by making $|R_S/Z_W| \rightarrow 0$. In practice, this is achieved by making the surface area of WE, A_W, much smaller than A_C, the area of CE. Another advantage of the technique that we adopt here is that the potentiostat performance becomes minimally sensitive to WE and RE interface electrostatics and drifts.

It is important to mention that the design of current sensors in the voltammetry system is challenging. The reason is the necessity to detect a very small I_x (pA range) in the presence of large background currents (nA range), specifically I_b and I_o, the offset currents of the detector.

D. System Specifications

In Table I, we list the key system level specifications that we are setting for this biochip. Besides the electro-chemical specifications required for voltammetry, we have set requirements that make the system compatible with DNA testing [24]. It is important to emphasize that the detection of up to 250 analytes enables new applications in MDx as it satisfies the multiplexing requirements of complex infectious disease, personalized medicine, and oncology tests [24]. Now, considering a practical number of biosensor replicates per analyte of 4, a ~1000-pixel biosensor array is required. A wide temperature range of operation is needed for polymerase chain reaction (PCR) amplification and melt curve analysis typically used in DNA based testing. 50 μL sample volume is typically obtained from conventional sample extraction workflow used in *in vitro* diagnostics (IVD). We intend to use a-C for implementing the electrodes, which is not only manufacturable and chemo-stable but also bio-compatible. To build a high-performance voltammetry assay, one requires a three-electrode voltammetry system with on-chip WE, RE, and CE [2]–[4], [12]. Furthermore, the WE has to be swept over a wide voltage range of ±0.75 V to accommodate a wide variety of redox labels for cyclic voltammetry (CV) scans. The detection circuitry should be capable of detecting a wide range of currents with a noise limit <0.5 pA. Such a low noise limit will enable CV scan rates of 0.1–1 V/s, where $I_x \sim$ 1–10 pA. Higher scan rates do not improve the signal-to-background performance since both I_x and I_b are linearly proportional to the CV scan rate [13]. The detection bandwidth of 50 Hz is chosen to capture all the non-linear components generated by the 1-V/s CV scan.

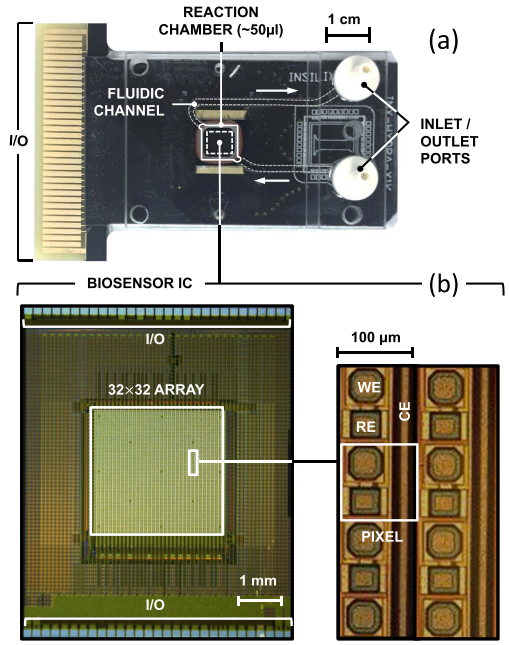

Fig. 3. (a) CMOS biochip module with fluidic cap. (b) Micrograph of the CMOS biochip with the pixel array.

III. SYSTEM IMPLEMENTATION

A. Biochip Module

In Fig. 3(a), we show the implemented biochip module that consists of the biosensor IC assembled onto a PCB substrate and encapsulated by a plastic flow through fluidic cap with

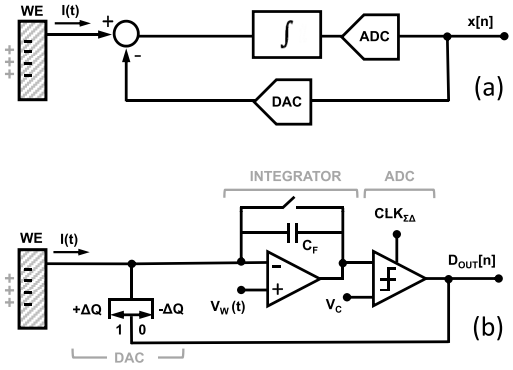

Fig. 4. (a) Block diagram of in-pixel $\Sigma\Delta$ modulator. (b) High-level circuit schematic.

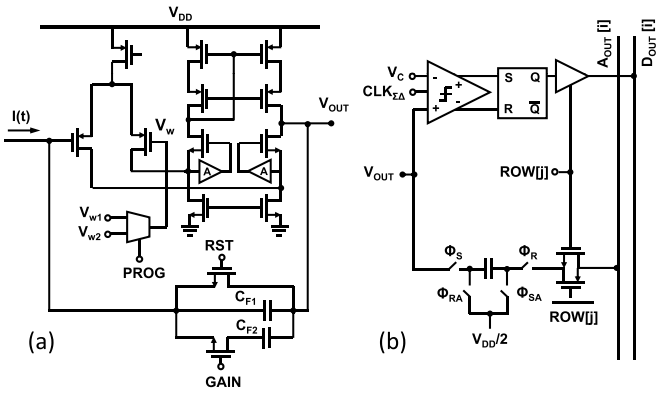

Fig. 5. Circuit schematic of the in-pixel. (a) Integrator. (b) 1-bit ADC.

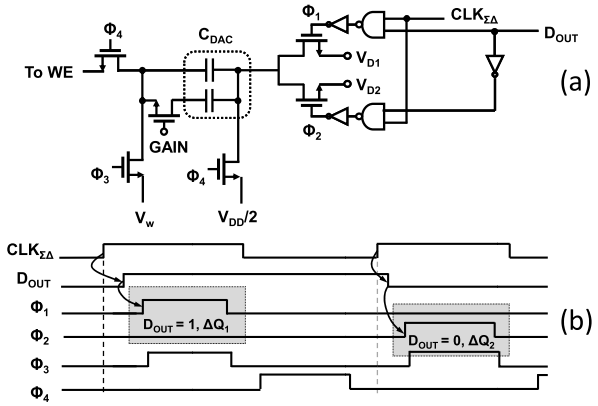

Fig. 6. Circuit schematic of (a) 1-bit DAC and (b) its switching waveform.

an inlet and outlet. The fluidic cap is designed to create a 50 μL reaction chamber on top of the biosensor IC and handle temperature up to 100 °C. The PCB substrate enables electrical connectivity and permits rapid heating/cooling by creating a low thermal resistivity contact from the substrate of the IC to an external (instrument) heatsink.

The IC [see Fig. 3(b)] includes a 32 × 32 array of biosensing pixels, each with three-electrode (WE, RE, and CE) connected to an embedded pixel voltammetry circuitry placed underneath them. Each pixel is 100 μm × 100 μm in size and the overall dimensions of the IC are 7 mm × 9 mm. The biochip is manufactured using a 0.25 μm 1P4M (one poly layer plus four interconnect metals) CMOS process.

B. Pixel Implementation

In each pixel, we implemented the first-order current sensing $\Sigma\Delta$ modulator [25], [26] connector to the WE transductor element, as shown in Fig. 4(a). The sensor input is the WE current $I(t) = I_x + I_b$, which is first fed into a high dc gain integrator, the output of which is quantized by the ADC to generate $D_{\rm OUT}$. This output controls a DAC, which performs the differentiation (Δ) operation.

The rationale behind using this sensor architecture was to enable the integration of a high DR (DR > 90 dB) sensor into a smaller pixel area when compared to other architectures, such as SAR, dual slope integration, or direct integration [3], [5]–[7]. Furthermore, the 1-bit digital output permits easy array-wide digital read out (scanning). The downside of this architecture is the need for high oversampling ratio (OSR) to achieve the required DR and the potential for idle tones when measuring low dc input currents. Due to our low detection bandwidth of 50 Hz, the first-order $\Sigma\Delta$ modulator with a clock frequency of 100 kHz suffices for our current detection range requirement of 0.5 pA–1 nA.

The high-level schematic of the pixel implementation is shown in Fig. 4(b). The integrator is implemented using a capacitive transimpedance amplifier (CTIA) with a feedback capacitor C_F. The CTIA also serves the purpose of setting the WE voltage to $V_W(t)$ for voltammetry. The ADC is implemented using a 1-bit clocked comparator, which compares the output of CTIA to an externally adjustable dc voltage V_C to generate the 1-bit output $D_{\rm OUT}$ with an oversampling clock $\rm CLK_{\Sigma\Delta}$. The DAC of this system is a switched-capacitor (S-C) charge subtraction circuit, which adds or subtracts a charge packet, ΔQ, from the charge stored in C_F, depending on output $D_{\rm OUT}$.

We show the detailed circuit schematic of the voltammetry pixel in Figs. 5 and 6. The CTIA [see Fig. 5(a)] uses a folded cascode gain-boosted OTA with a high open-loop gain (A_v > 94 dB) and wide gain bandwidth product (GBW ≥ 30 MHz). This topology and performance specifications were chosen to ensure functionality in the presence of large and varying WE capacitance $C_W \approx C_H C_D/(C_H + C_D)$ (typically 100 pF–1 nF), specifically, to adequately settle $V_{\rm OUT}$ within a few microseconds during the $\Sigma\Delta$ operation of the sensor. Also, high gain is essential to reduce any non-linear $V_{\rm OUT}/A$ component at the input.

At the OTA input, we use large input transistor pairs (W/L = 64/1.5 μm) to diminish the input offset voltage, V_o, below 1 mV and minimize the 1/f noise as well. The NMOS cascode stage is gain boosted [27] to overcome the loading effect of the large input transistors and to match the PMOS and NMOS load resistances to meet A_v > 94 dB. It is important to mention here that chopper circuits are commonly used to reduce the input 1/f and attenuate the offset [28]. However, their adoption in small area footprint, single-ended voltammetry sensors is not recommended due to the large ripple currents involved, which require additional circuitry to compensate. Due to large input electrode–electrolyte capacitance (C_W), the peak ripple current can be as high as 1 nA.

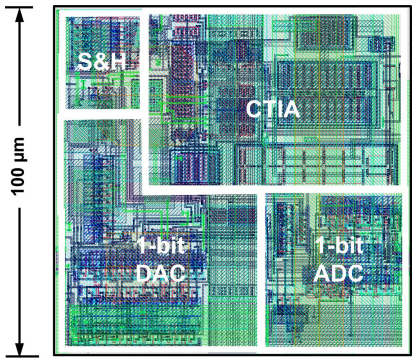

Fig. 7. Pixel layout.

The OTA accommodates a wide input common mode range of ±0.75 V around $V_{DD}/2 = 1.25$ V. It is possible to set V_W to one of the two externally generated voltages of V_{W1} or V_{W2}, using the program signal (PROG). The feedback capacitor of the OTA (implemented using MIM capacitors) can be changed between 200 and 500 fF by using the GAIN mode switches. This allows changing the feedback gain by changing C_F.

The 1-bit ADC [see Fig. 5(b)] is a Yukawa [29] clocked comparator and compares V_{OUT} with V_C at the rising edge of $CLK_{\Sigma\Delta}$, operating nominally at 100 kHz. The output of the comparator is captured using an S-R latch and placed on the column line $D_{OUT}[i]$ through a tristate buffer that is controlled by the ROW[j] signal. For testability and characterization, we placed an analog sampling circuit in every pixel to capture the output of the OTA, V_{OUT}, and transfer it onto the analog column line column $A_{OUT}[i]$.

The 1-bit DAC is designed using the S-C circuit of Fig. 6. Multiple clock phases, ϕ_{1-4}, are derived from $CLK_{\Sigma\Delta}$. During the first phase, the charge corresponding to either $V_{D1} - V_W$ or $V_{D2} - V_W$ ($\Delta V \sim \pm 0.5$ V) is stored onto C_{DAC}, the charge storage capacitor, depending on D_{OUT}. During the second phase, this stored charge is transferred onto C_F to perform the charge subtraction (Δ operation). C_{DAC} can be set to either 100 or 250 fF using the GAIN mode signal.

The maximum current that can be detected by pixel circuitry, I_{max}, is given by

$$I_{max} = \Delta Q \times f_{\Sigma\Delta} = C_{DAC} \times \Delta V \times f_{\Sigma\Delta}. \quad (6)$$

For $\Delta V = 0.5$ V and in nominal oversampling conditions and low GAIN mode, I_{max} becomes ±12.5 nA. The offset current, I_o, varies from pixel to pixel as it is a function of V_{os} in the form of

$$I_o = C_{DAC} \times V_o \times f_{\Sigma\Delta}. \quad (7)$$

In Fig. 7, we show the pixel layout. One key challenge was to integrate the entire pixel circuitry into the 100 μm × 100 μm area. As evident, a large percentage of the area (~38%) is occupied by the integrator (top right) with its large input pair and the digital logic for generating all the switching signals necessary for the 1-bit DAC (~32%) (bottom left).

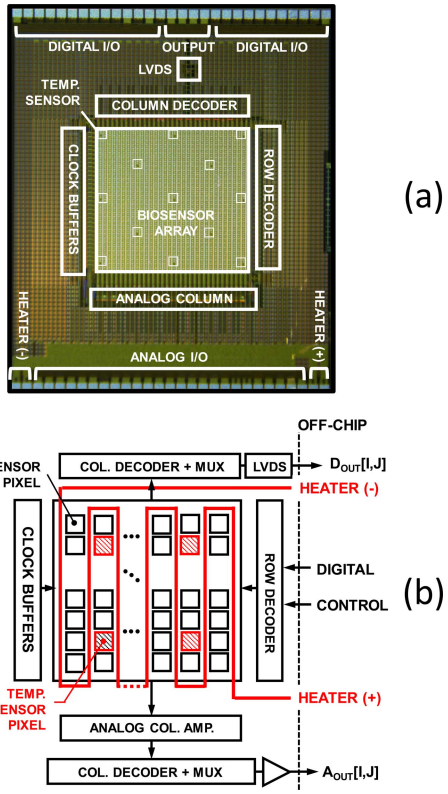

Fig. 8. Biochip IC. (a) Micrograph. (b) Architecture.

C. Array Level Architecture

The top-level chip architecture along with the chip micrograph is shown in Fig. 8. The biochip array consists of 32 × 32 pixels, where 13 are temperature sensor pixels. These pixels measure the temperature profile of the biochip at different coordinates and have the same circuitry as voltammetry pixels. However, their input is connected to a reverse-biased n-well/p_{sub} diode (covered with metal to protect from ambient light) instead of a WE to measure the dark current, I_{dc}, of the diodes, which is a good measurand for temperature [30], and is given by

$$I_{dc}(T) = I_0 e^{-(E_g/nkT)} \quad (8)$$

where I_0 is a constant, E_g is the bandgap activation energy, n is a number between 1 and 2, k is Boltzmann's constant, and T is the absolute temperature.

As shown in Fig. 8, each pixel can be individually addressed using the row and column decoders and $D_{OUT}[i, j]$ is read sequentially and sent off-chip to an FPGA using a low-voltage differential signaling (LVDS) scheme. For $f_{\Sigma\Delta} = 100$ kHz, the pixels are read serially using 102.4-MHz clock to enable synchronous readout of the entire array frame. The array readout happens at much faster rate than the CV scan rate (0.1–1 V/s). The oversampling clock $CLK_{\Sigma\Delta}$ is buffered using the clock buffers' block and sent to the entire array. During test and characterization, $V_{OUT}[i, j]$ is sent off-chip using the analog scan chain, which includes analog column amplifier circuitry.

The chip also includes a heater line, which is built using a serpentine structure in the top metal layer spread throughout

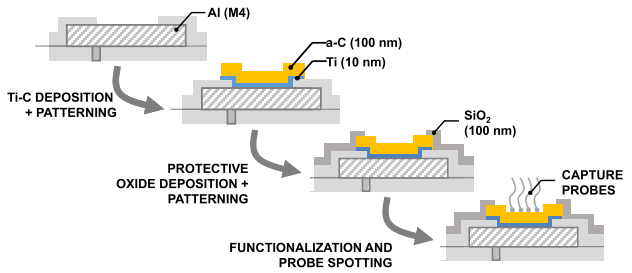

Fig. 9. Wafer-level a-C electrode fabrication process.

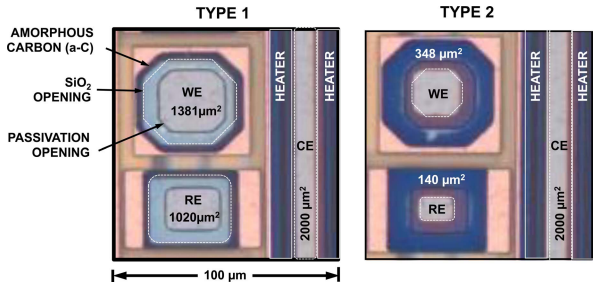

Fig. 10. Pixel micrograph with the working, reference, and counter electrodes.

the entire array. The heater line has a total resistance of 2 Ω and provides up to 5 W of power. The peak current is ∼2 A with the electro-migration mean time between failures (MTBF) of 10 000 h, which is acceptable for this one-time-use biochip. The combination of heater line and on-chip temperature sensor permits closed-loop temperature control, which is essential in molecular sensing applications.

D. Electrode Manufacturing

We chose a-C as the electrode material because a-C is chemically and thermally stable over a wide range of operating conditions [16]. In addition, we can covalently attach capturing probes and molecular linkers to a-C, which is not possible for precious metal (Au and Pt) electrodes [30], [31].

The electrode fabrication process is shown in Fig. 9. WE, RE, and CE are all created over the exposed top metal layer (M4) of the CMOS IC. To do this, the CMOS wafers are first subject to sputtering and patterning of a-C along with the Ti adhesion layer. The average thickness of the a-C/Ti layer is 116 ± 4 nm. To protect the exposed Ti edges from chemical erosion, a protective layer of SiO_2 is deposited and patterned. The thickness of SiO_2 is approximately 100 nm.

We implemented two different types of pixels (see Fig. 10) to test different electrode areas and step coverages. Pixel Type 1 has larger area WE and RE when compared with pixel Type 2, while CE area is the same for the pixels.

In this system, the RE and CE of all the individual pixels are tied together to create one global RE and CE for the chip driven using an off-chip potentiostat. These electrodes have much larger area than the working electrodes, which, as discussed before, offer a more accurate voltammetry system. The distributed RE and CE create a uniform electric field across the entire array. The global RE and CE are driven using an off-chip potentiostat.

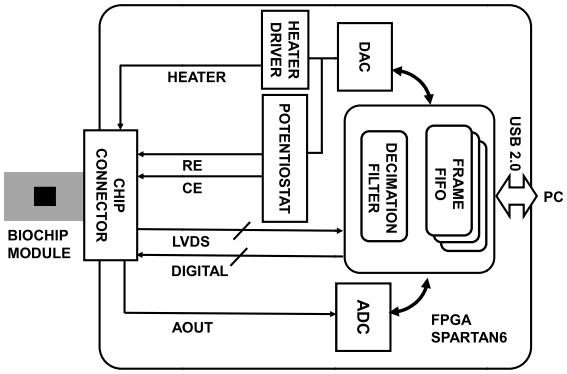

Fig. 11. Block diagram of the electronics board used in the measurement setup.

E. Surface Bio-Functionalization

To bio-functionalize a-C surfaces, we first plasma treat it to partially oxidize the exposed a-C material and produce available carboxylate groups. For DNA probe immobilization, N-hyroxysulfosuccinimide (10 mM) and 1-ethyl-3-(3-dimethylaminopropyl)-carbodiimide (100 mM) were combined with 5′-amino terminated oligonucleotide probe (100 μM) and contacted with the array surface. After 60 min, the surface is thoroughly washed to remove unbound reagents and finally dried. Such a functionalization scheme provides a stable covalent attachment of probes to the electrode surface.

IV. Measurement Results

A. Measurement Setup

The measurement setup makes use of a reader electronics board (see Fig. 11), which consists of a SPARTAN6 FPGA core. The FPGA performs: 1) generation of all digital signals required for biochip operation; 2) array level decimation filtering of 1-bit pixel data using 1024 digital sinc^2 filters; 3) buffering of frames using an FIFO; 4) communication with an external computer using a USB interface; and 5) control/reading of DAC/ADC channels.

The reader electronics board also includes a heater driver to drive current into the on-chip heater. Combined with the data from the on-chip temperature sensor, the board can perform closed-loop temperature control. The board also includes potentiostat circuitry to perform three-electrode voltammetry using the on-chip RE and CE.

B. Electrical Measurements

We first measured the electronic performance of the pixel with 100-mM KCl electrolyte present under $V_W = 0$ conditions. This setup was selected to ensure that the effects of C_W and the electrolyte resistance are captured in the measurements.

Fig. 12 reports the histogram of the measured offset current of 1011 pixels of a single chip. The standard deviation of I_o of 100-pA rms $= 0.01 I_{\max}$, hence it does not affect the DR and can be easily subtracted.

Fig. 13 shows the input-referred noise spectrum of the pixel in 100-mM KCl solution at 0-V dc bias ($V_W = 1.25$ V

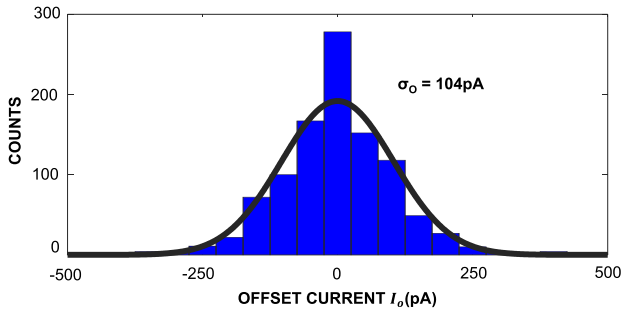

Fig. 12. Histogram of measured pixel offset currents.

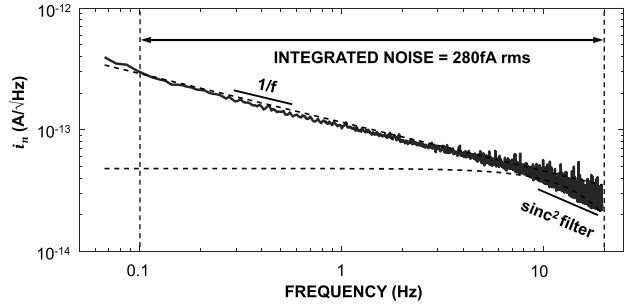

Fig. 13. Measured pixel noise performance.

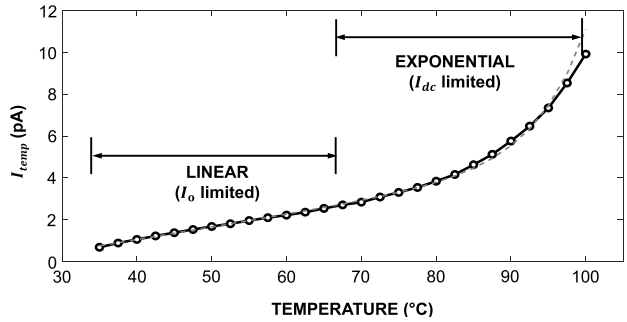

Fig. 14. Measured temperature sensor response.

and $V_R = 1.25$ V). The noise spectrum shown is the average of all the pixels with the larger WE (1381 μm^2). As evident, the dominant component is the 1/f noise, which originates from the OTA noise and is amplified by the large C_W. It is a key to recognize that the quantization noise is made negligible by using a large OSR (OSR $>$ 2000). The noise performance is dominated by 1/f noise, which is significant between 0.1 and 10 Hz. Any increase in BW up to 50 Hz does not affect the noise performance ($<$1% contribution). The integrated noise is 280 fA rms, which considering $I_{\max} = 12.5$ nA results in a detection DR of 93 dB.

We show the performance of the temperature sensor pixels measured in Fig. 14. At lower temperatures, the linear variation of I_o is observed. However, at higher temperatures, the exponential effect of $I_{\rm dc}$ according to (8) becomes dominant. The temperature sensor has the noise-limited resolution of 0.75 °C between 40 and 70 °C in the linear offset limited region and $<$0.5 °C in the dark current limited region beyond 70 °C.

Next, we subject the biochip to a CV sweep using the three-electrode setup, and V_W is subject to a saw tooth waveform

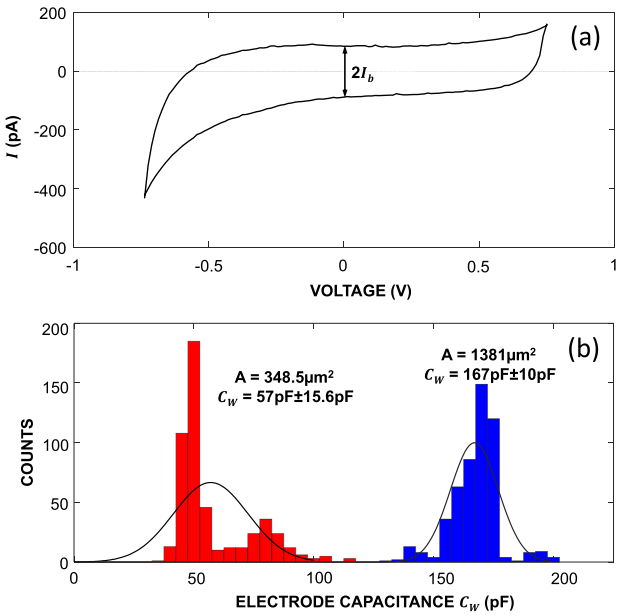

Fig. 15. (a) Voltammetry plot showing the background current using larger WE. (b) Histogram of working electrode capacitances.

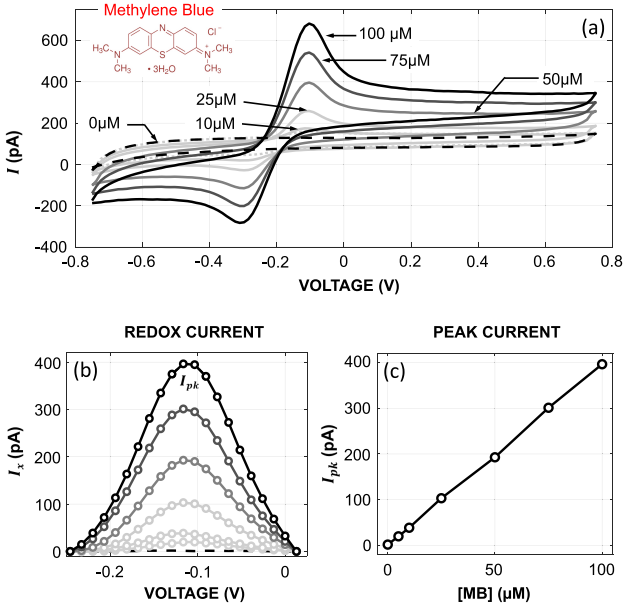

Fig. 16. Redox label (MB) measurements. (a) Total current measured. (b) Redox current versus swept voltage. (c) Peak current versus concentration.

with the rate of 0.5 V/s. As evident in Fig. 15(a), I_b is 150 pA, which can be easily accommodated within DDR of the pixel. C_W is measured at 0-V bias and its histogram is reported in Fig. 15(b). Type 1 pixels (a-C WE area of 1381 μm^2) had $C_W = 167 \pm 10$ pF ($\mu \pm \sigma$), while Type 2 pixels (a-C WE area of 348.5 μm^2) had $C_W = 57.6$ pF $\pm$ 15.6 pF ($\mu \pm \sigma$).

C. Redox Label Measurements

We took advantage of a widely used redox molecule (methylene blue (MB)) [20], [21] to characterize the generation of I_x. MB is a widely used label for DNA biosensing

TABLE II
DNA SEQUENCES USED IN BIO-EXPERIMENTS

Sequence Name	Sequence
Probe	5'-NH_2-$(CH_2)_6$-GCAGTATCTTCTATTTCTCCACACTGC-**MB**-3'
Target	5'-GCAGTGTGGAGAAATAGAAGATACTGC-3'
Negative Control	5'-NH_2-$(CH_2)_6$-CGCGATAGAAGAACTGGCGCTCCGTGTGATCGCG-**MB**-3'

* MB: Methylene Blue

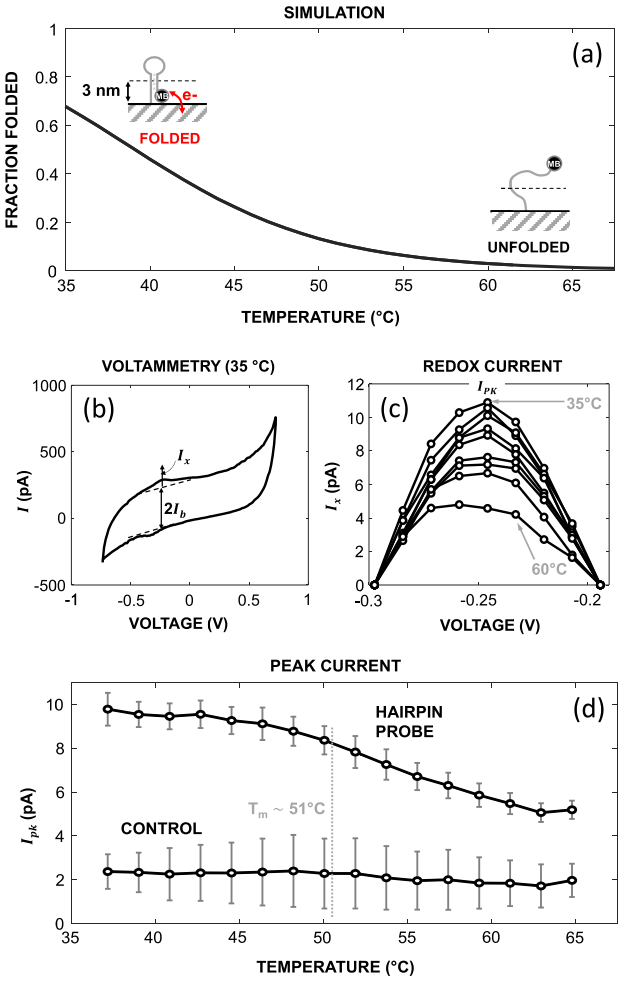

Fig. 17. Biological experiments with DNA folded loop structure. (a) Simulation results for a folded loop structure. (b) Voltammetry plot at 35 °C. (c) Redox current plots at different temperatures. (d) Peak current versus temperature showing the hairpin probe and control pixels.

with $V_{ox} = 0.2$ V. We first performed measurements with varying concentration of MB (0–100 μM) in the electrolyte to study the response of the voltammetry pixel. Fig. 16(a) reports the overall current measured, which clearly includes the I_x peak in addition to I_b. Next, we extract these peaks and generate the I_x waveforms around V_{ox} [see Fig. 16(b)], which is a unique characteristic of MB. The linear slope of the peak current versus concentration is shown in Fig. 16(c), demonstrating ~4-pA/μM transduction gain based on the first-order fit [I_{pk}(pA) = 3.96 [$C(\mu M)$] + 0.4622, $R^2 = 0.9995$].

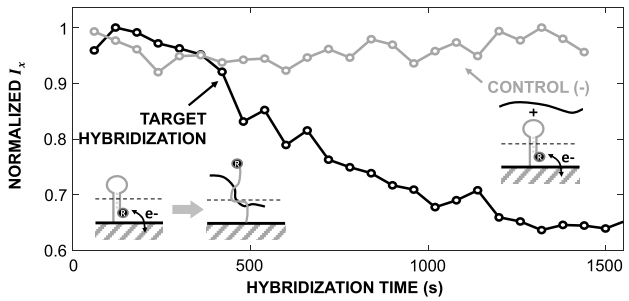

Fig. 18. Biological experiments with DNA target hybridization along with the negative control.

TABLE III
PERFORMANCE COMPARISON

Parameter	JSSC 2004 [2]	JSSC 2008 [3]	JSSC 2014 [5]	This work
Sensor Signal Chain	Current-to-Frequency Converter	CTIA + Dual Slope ADC	Current Conveyer + Dual Slope ADC	ΣΔ Current Detector
Process Technology (μm)	0.5	0.25	0.13	0.25
Supply Voltage (V)	5	2.5	1.2	2.5
Pixel Area (μm^2)	100,000+	250,000+	60,000	10,000
Electrode Material	Ti/Pt/Au	Ti/Au	Ni/Pd/Au	Ti/C
Number of Pixels	128	16	54	1024
I_{max} (nA)	100	250	2.2, 59, 350	12.5
Sensitivity (pA)	10	240	8.6, 132, 1050	0.28
Dynamic Range (dB)	80	60	48, 53, 51+	93
Readout Speed (Hz)	7	2500	3400	50
Power (mW)	-	10+	0.042/pixel	0.25/pixel
Integrated Heater and Temperature Sensor	No	No	No	Yes
Integrated Potentiostat	Yes	Yes	Yes	No

+ Estimated

D. Biological Measurements

To demonstrate the use of our CMOS biochip for biosensing, we performed multiple DNA testing experiments, which we discuss in this section.

First, we took advantage of folded DNA loop structures (hairpin probes) attached to the surface that can act as temperature switches. The detailed DNA sequences used in the measurements are provided in Table II. The probe has an MB label at its end, which, at low temperature, remains through DNA hybridization within the tunneling distance of the a-C electrode surface and generates I_x. At higher temperature, the loop opens up, the MB moves outside the tunneling distance, and the signal fades.

In Fig. 17(a)–(d), we report both the simulation and measurement results obtained from biochip for the heat switching phenomenon. The pixels are subject to voltage sweep of ±0.75 V at 0.5 V/s in a buffer containing 25-mM Tris-HCl (pH 8 at 25 °C), 55-mM NaCl, and 3.5-mM $MgCl_2$. The temperature is swept between 35 and 80 °C. The voltammetry plot at 35 °C clearly shows the presence of I_x due to the folded loop structure [see Fig. 17(b)]. The observed I_x drops as temperature increases as expected [see Fig. 17(c)]. The peak of I_x [see Fig. 17(d)] shows a characteristic drop with temperature (also known as "melting" characteristic) and reaches its 50% point close to 51 °C. This is in contrast to the negative control pixel where no DNA probe is immobilized where little or no changes in I_x is measured. The variation (∼10%) observed across the measured $N = 12$ pixels which we believe originates from the variation in electrode area and in surface probe density. The control probe shows the drift associated with the melt curve measurement, which was taken over a 15-min period.

Next, we took advantage of the system to detect DNA targets present in the electrolyte using a label-free detection technique [20], [21]. In this case, experiments are done with two different probe sequences: one acting as the positive and one acting as the negative control at 35 °C hybridization temperature. As shown in Fig. 18, when 100 nM of the target is added to the reaction, I_x drops as expected at the positive control pixels since probe-target binding pushes MB label away from the surface. This is in contrast with the negative control pixels where no change is observed.

V. Conclusion

The advent of a fully integrated, manufacturable, low-cost, and versatile electronic biosensor will be revolutionary in MDx and related fields. In this article, we report a successful design and implementation of a CMOS biochip that moves toward this goal with performance approaching that of optical biosensors. Compared with the previously reported electrochemical biosensors (see Table III), this biochip offers a higher DR and sensitivity, while employing electrode transducer structures and materials that are readily manufacturable and provide the required surfaces for the bio-functionalization processes.

There remain significant challenges that future work should address. For example, the background in voltammetry is still too high and with its inherently single-ended nature, it is difficult to detect analytes with lower concentration than what is reported. One technique to overcome this high background is to use a differential system to cancel the background current. However, this method will be limited by the electrode capacitance variation. Another method is to make use of correlated double sampling (CDS) techniques with the background sample taken away from redox potential (V_{ox}) to measure I_b and then to subtract it from another sample taken at V_{ox} to measure I_x. Another challenge is the variation in surface probe density and electrode surface area, which requires further improvements in the areas of surface chemistry for functionalization of a-C electrodes and in surface fabrication techniques, which is well beyond the scope of this article.

The most expensive aspect of commercialization of biochip devices is the integration of the fluidics into the CMOS biochips. The fluidic integration needs to be cost efficient and standardized for mainstream use.

References

[1] J. Wang, "Electrochemical biosensors: Towards point-of-care cancer diagnostics," *Biosens. Bioelectron.*, vol. 21, no. 10, pp. 1887–1892, Apr. 2006.

[2] M. Schienle *et al.*, "A fully electronic DNA sensor with 128 positions and in-pixel A/D conversion," *IEEE J. Solid-State Circuits*, vol. 39, no. 12, pp. 2348–2445, Dec. 2004.

[3] P. M. Levine, P. Gong, R. Levicky, and K. L. Shepard, "Active CMOS sensor array for electrochemical biomolecular detection," *IEEE J. Solid-State Circuits*, vol. 43, no. 8, pp. 1859–1871, Aug. 2008.

[4] C. Yang, Y. Huang, B. L. Hassler, R. M. Worden, and A. J. Mason, "Amperometric electrochemical microsystem for a miniaturized protein biosensor array," *IEEE Trans. Biomed. Circuits Syst.*, vol. 3, no. 3, pp. 160–168, Jun. 2009.

[5] H. M. Jafari, K. Abdelhalim, L. Soleymani, E. H. Sargent, S. O. Kelley, and R. Genov, "Nanostructured CMOS Wireless Ultra-Wideband Label-Free PCR-Free DNA Analysis SoC," *IEEE J. Solid-State Circuits*, vol. 49, no. 5, pp. 1223–1241, May 2014.

[6] C.-L. Hsu, A. Sun, Y. Zhao, E. Aronoff-Spencer, and D. A. Hall, "A 16×20 electrochemical CMOS biosensor array with in-pixel averaging using polar modulation," in *Proc. IEEE Custom Integr. Circuits Conf. (CICC)*, Apr. 2018, pp. 1–4.

[7] J. M. Rothberg *et al.*, "An integrated semiconductor device enabling non-optical genome sequencing," *Nature*, vol. 475, no. 7356, pp. 348–352, Jul. 2011.

[8] B. Jang, P. Cao, A. Chevalier, A. Ellington, and A. Hassibi, "A CMOS fluorescent-based biosensor microarray," in *IEEE ISSCC Dig. Tech. Papers*, Feb. 2009, pp. 436–437.

[9] D. E. Schwartz, E. Charbon, and K. L. Shepard, "A single-photon avalanche diode array for fluorescence lifetime imaging microscopy," *IEEE J. Solid-State Circuits*, vol. 43, no. 11, pp. 2546–2557, Nov. 2008.

[10] L. Hong, H. Li, H. Yang, and K. Sengupta, "Fully integrated fluorescence biosensors on-chip employing multi-functional nanoplasmonic optical structures in CMOS," *IEEE J. Solid-State Circuits*, vol. 52, no. 9, pp. 2388–2406, Sep. 2017.

[11] B. Jang and A. Hassibi, "Biosensor systems in standard CMOS processes: Fact or fiction?" *IEEE Trans. Ind. Electron.*, vol. 56, no. 4, pp. 979–985, Apr. 2009.

[12] A. J. Bard, L. R. Faulkner, J. Leddy, and C. G. Zoski, *Electrochemical Methods: Fundamentals and Applications*, vol. 2. New York, NY, USA: Wiley, 1980.

[13] S. D. O'Connor, G. T. Olsen, and S. E. Creager, "A Nernstian electron source model for the AC voltammetric response of a reversible surface redox reaction using large-amplitude AC voltages," *J. Electroanal. Chem.*, vol. 466, no. 2, pp. 197–202, May 1999.

[14] J. Wang, "Electrochemical nucleic acid biosensors," *Anal. Chim. Acta*, vol. 469, no. 1, pp. 63–71, Sep. 2002.

[15] A. Manickam, R. Singh, S. Ayazian, and A. Hassibi, "Front-end integrated circuits for high-performance biological and chemical sensing," in *Proc. IEEE 54th Int. Midwest Symp. Circuits Syst. (MWSCAS)*, Aug. 2011, pp. 1–4.

[16] R. L. McCreery, "Advanced carbon electrode materials for molecular electrochemistry," *Chem. Rev.*, vol. 108, no. 7, pp. 2646–2687, Jun. 2008.

[17] N. Garg, E. Carrasquillo-Molina, and T. R. Lee, "Self-assembled monolayers composed of aromatic thiols on gold: Structural characterization and thermal stability in solution," *Langmuir*, vol. 18, no. 7, pp. 2717–2726, Mar. 2002.

[18] F. Domengie, P. Morin, and D. Bauza, "Modeling the dark current histogram induced by gold contamination in complementary-metal-oxide-semiconductor image sensors," *J. Appl. Phys.*, vol. 118, no. 2, Jul. 2015, Art. no. 024501.

[19] J. S. Daniels and N. Pourmand, "Label-free impedance biosensors: Opportunities and challenges," *Electroanalysis*, vol. 19, no. 12, pp. 1239–1257, Jun. 2007.

[20] D. Kang, X. Zuo, R. Yang, F. Xia, K. W. Plaxco, and R. J. White, "Comparing the properties of electrochemical-based DNA sensors employing different redox tags," *Anal. Chem.*, vol. 81, no. 21, pp. 9109–9113, Oct. 2009.
[21] F. Ricci and K. W. Plaxco, "E-DNA sensors for convenient, label-free electrochemical detection of hybridization," *Microchimica Acta*, vol. 163, nos. 3–4, pp. 149–155, Oct. 2008.
[22] M. M. Ahmadi and G. A. Jullien, "Current-mirror-based potentiostats for three-electrode amperometric electrochemical sensors," *IEEE Trans. Circuits Syst. I, Reg. Papers*, vol. 56, no. 7, pp. 1339–1348, Jul. 2009.
[23] J. Zhang, Y. Huang, N. Trombly, C. Yang, and A. Mason, "Electrochemical array microsystem with integrated potentiostat," in *Proc. IEEE Sensors*, Oct./Nov. 2005, p. 4.
[24] A. Hassibi *et al.*, "Multiplexed identification, quantification and genotyping of infectious agents using a semiconductor biochip," *Nature Biotechnol.*, vol. 36, no. 8, pp. 738–745, Jul. 2018.
[25] R. Schreier and G. C. Temes, *Understanding Delta-Sigma Data Converters*, vol. 74. Piscataway, NJ, USA: IEEE Press, 2005.
[26] B. E. Boser and B. A. Wooley, "The design of sigma-delta modulation analog-to-digital converters," *IEEE J. Solid-State Circuits*, vol. 23, no. 6, pp. 1298–1308, Dec. 1988.
[27] K. Bult and G. J. G. M. Geelen, "A fast-settling CMOS op amp for SC circuits with 90-dB DC gain," *IEEE J. Solid-State Circuits*, vol. 25, no. 6, pp. 1379–1384, Dec. 1990.
[28] C. C. Enz and G. C. Temes, "Circuit techniques for reducing the effects of op-amp imperfections: Autozeroing, correlated double sampling, and chopper stabilization," *Proc. IEEE*, vol. 84, no. 11, pp. 1584–1614, Nov. 1996.
[29] A. Yukawa, "A CMOS 8-bit high-speed A/D converter IC," *IEEE J. Solid-State Circuits*, vol. JSSC-20, no. 3, pp. 775–779, Jun. 1985.
[30] S. M. Sze and K. N. Kwok, *Physics of Semiconductor Devices*. Hoboken, NJ, USA: Wiley, 2006.
[31] M. Rosso *et al.*, "Covalent attachment of organic monolayers to silicon carbide surfaces," *Langmuir*, vol. 24, no. 8, pp. 4007–4012, Mar. 2008.

Arun Manickam (M'16) received the B.S. degree from the College of Engineering, Guindy, Anna University, Chennai, India, in 2002, and the M.S. and Ph.D. degrees from The University of Texas at Austin, Austin, TX, USA, in 2008 and 2012, respectively, all in electrical engineering.

He has held engineering positions at Qualcomm, San Diego, CA, USA, Silicon Laboratories Inc., Austin, and Bosch Research and Technology Center, Palo Alto, CA, USA, in 2007, 2008, and 2010, respectively. He co-founded InSilixa Inc., Sunnyvale, CA, USA, a CMOS biochip company, where he has been working on developing point-of-care (POC) platforms for medical diagnostic testing, by leveraging semiconductor-based CMOS biochip technology. He is currently employed as the Director of Engineering. He has 12 publications and holds five patents in the area of CMOS biosensors.

Kae-Dyi You received the B.S. degree in electrical engineering from National Cheng Kung University, Tainan, Taiwan, in 2006, and the M.S. degree in electrical engineering from National Chiao Tung University, Hsinchu, Taiwan, in 2009. He is currently pursuing the Ph.D. degree in electrical and computer engineering with New York University (NYU), New York, NY, USA.

From 2009 to 2016, he was an Analog and Mixed-Signal IC Design Engineer in Taiwan, where he was involved in full chip design and mass production of three main projects: fingerprint sensing front-end circuits, advanced audio codec systems, and the design of high-speed serial link ICs. His current research interests include design and implementation of power and area-efficient CMOS read-out circuits for brain interfaces and heterogeneous biosensing microsystems.

Nicholas Wood received the B.S. degree in electrical engineering from The University of Texas at Austin, Austin, TX, USA, in 2013, and the M.S. degree in electrical engineering from The University of Texas at Dallas, Richardson, TX, USA, in 2016.

He is currently a Staff Engineer with InSilixa Inc., Sunnyvale, CA, USA, specializing in embedded systems and software for CMOS biochips and biomedical instrumentation.

Lei Pei received the B.S. and M.S. degrees in chemistry from Nankai University, Tianjin, China, in 2001 and 2004, respectively, and the Ph.D. degree in analytical chemistry from Brigham Young University, Provo, UT, USA, in 2011.

He continued to work as a Post-Doctoral Fellow with Brigham Young University until 2013. He was a Post-Doctoral Fellow with Johns Hopkins University, Baltimore, MD, USA, from 2013 to 2015. He is currently a Senior Scientist with InSilixa Inc., Sunnyvale, CA, USA, where he is involved in the development of surface modification, chemical processing, and analysis.

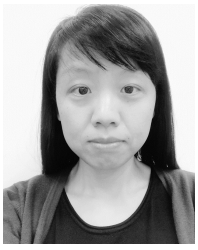

Yang Liu received the B.S. degree in chemistry from Nankai University, Tianjin, China, in 2001, and the Ph.D. degree in organic chemistry from Brigham Young University, Provo, UT, USA, in 2010.

She was with the lab of Brigham Young University as a Post-Doctoral Fellow until 2011. Her project was the synthesis of glycolipids and evaluation of their NKT cell stimulatory properties. She joined the Center for Biomarker Discovery, Johns Hopkins University, Baltimore, MD, USA, in 2015, with a focus on the method development of the selected reaction monitoring (SRM) technique for protein quantification. She has been a Scientist with InSilixa Inc., Sunnyvale, CA, USA, since 2017. Her current research interest includes method development of the protein microarray.

Rituraj Singh received the B.Tech. degree in electrical engineering from IIT Kanpur, Kanpur, India, in 2005, the M.S. degree in electrical and computer engineering from the University of Toronto, Toronto, ON, Canada, in 2009, and the Ph.D. degree in electrical and computer engineering from The University of Texas at Austin, Austin, TX, USA, in 2013.

He has held engineering positions with Texas Instruments, Bengaluru, India, Mentor Graphics, Noida, India, and Silicon Laboratories Inc., Austin, in 2004, from 2005 to 2006, and in 2010, respectively. He was with InSilixa Inc., Sunnyvale, CA, USA, from 2012 to 2017, where he was a member of the co-founding team. His research interests include circuits and systems for biological, medical, and consumer sensory applications.

Dr. Singh was a recipient of the Proficiency Medal for the best B.Tech. project in electrical engineering at IIT Kanpur in 2005.

Nader Gamini received the B.S. degree in computer science from California State University at East Bay, Hayward, CA, USA, in 1984, and the M.B.A. degree from the UCLA Anderson's School of Management, Los Angeles, CA, USA, but left the program to launch his first start-up.

He was the Vice President of the Manufacturing of the PLP Division of NetLogic Microsystems, Santa Clara, CA, USA, and the Chief Operating Officer and the Co-Founder of Aeluros, Mountain View, CA, USA. Before Aeluros, he was an executive of several companies, such as Rambus, Mountain View, and Sirenza Microdevices, Sunnyvale, CA, USA. He currently serves as a Chief Operating Officer and a Board Member of InSilixa Inc., Sunnyvale. He has served on the boards of Directors of four companies, and has been an Advisor to many companies in biotech, wireless communications, medical devices, solar, MEMS, optics, and other related industries. He has over 35 years of experience in high-volume, global manufacturing of electronics for commercial, military, and medical applications. He has nine issued patents in the areas of high-performance semiconductor packaging and module technologies.

Mark W. McDermott (S'75–M'78–LM'14) received the B.S. degree from The University of New Mexico, Albuquerque, NM, USA, in 1977, and the M.S. and Ph.D. degrees from The University of Texas at Austin, Austin, TX, USA, in 1988 and 2014, respectively, all in electrical engineering.

He has 40 years of industry experience in the product development of silicon systems. This includes the Senior Director at Apple Inc., Austin, the Vice President/General Manager at Intrinsity Inc., Austin, and the Director/ General Manager at Intel Corporation, Austin. He is currently a Professor of Practice with the Electrical and Computer Engineering Department, The University of Texas at Austin, and a Technical Advisor with Insilxa Inc., Sunnyvale, CA, USA. He holds 19 patents and has 15 publications in the areas of VLSI design, engineering education, and engineering management.

Dr. McDermott is a member of the Association for Computing Machinery and the Texas Society of Professional Engineers.

Davood Shahrjerdi (SM'16) received the Ph.D. degree in solid-state electronics from The University of Texas at Austin, Austin, TX, USA, in 2008.

He was with the IBM Thomas J. Watson Research Center, Yorktown Heights, NY, USA. He is currently an Assistant Professor of electrical and computer engineering with New York University (NYU), New York, NY, USA. His research explores the science and technology of emerging nanomaterials and devices and their interfaces with silicon CMOS.

Dr. Shahrjerdi was a recipient of the IBM Outstanding Technical Achievement Award and the IBM Master Inventor.

Robert G. Kuimelis received the B.S. degree in chemistry from the Saint Mary's College of California, Moraga, CA, USA, in 1989, and the Ph.D. degree in organic chemistry from the University of California at Davis, Davis, CA, USA, in 1993.

He was a Post-Doctoral Fellow with the Boston College, Chestnut Hill, MA, USA, from 1994 to 1996, focusing on non-natural nucleic acids and catalytic RNA mechanism. From 1996 to 1997, he was with Applied Biosystems, Foster City, CA, USA. From 1997 to 2002, he was with Phylos, Lexington, MA, USA. From 2002 to 2011, he was with Affymetrix, Santa Clara, CA, USA, as the Director of chemistry. From 2012 to 2015, he was with HealthTell, Chandler, AZ, USA, as the Senior Director of chemistry. Since 2015, he has been with InSilixa Inc., Sunnyvale, CA, USA, as the Vice President of chemistry. He has authored several book chapters and many published articles in the areas of nucleic acid chemistry and biophysics, surface chemistry, and DNA/peptide/protein microarrays. He holds 30 issued U.S. patents. His scientific interests are at the interface of chemistry, biology, and technology and the development of innovative platforms with broad potential to impact health.

Dr. Kuimelis is a member of the American Chemical Society.

Arjang Hassibi (S'99–M'05–SM'10) received the B.S. degree (Hons.) from the University of Tehran, Tehran, Iran, in 1997, and the M.S. and Ph.D. degrees in electrical engineering from Stanford University, Stanford, CA, USA, in 2001 and 2005, respectively.

He attended the post-doctoral training at the California Institute of Technology (Caltech), Pasadena, CA, USA. He has held various research and development positions in industry and academia, including second lieutenant with the Iranian Army Research Center, Tehran, from 1997 to 1999, the Stanford Microwave Integrated Circuits (SMIrC) Laboratory, Stanford, from 1999 to 2005, the Stanford Genome Technology Center, Stanford, from 2001 to 2003, the CMOS High-Speed Integrated Circuits (CHIC) Laboratory, Caltech, from 2005 to 2006, and Xagros Genomics, Sunnyvale, CA, USA, a start-up company, which he co-founded in 2001. He was a Faculty Member with the Electrical and Computer Engineering Department and the Institute for Cellular and Molecular Biology, The University of Texas at Austin, Austin, TX, USA, from 2006 to 2011, and a Visiting Professor with IBM Research at Yorktown, Yorktown Heights, NY, USA, from 2010 to 2011. Most recently, he was the Healthcare Thrust Lead with the Semiconductor Research Corporation (SRC), Durham, NC, USA. He has been the CEO and Founder of InSilixa Inc., Sunnyvale, since 2012. His current research interests include intersection of biotechnology and engineering, specifically biosensors and bioelectronics, biomedical electronics, and integrated sensors.